UNIVERSITY OF ATHENS
Faculty of Geology and Geoenvironment
Department of Geophysics and Geothermics

KNOWLEDGE FOR THE FUTURE
Joint Assembly Gothenburg IAHS - IAPSO - IASPEI Sweden 22-26 July 2013
constituent Associations of International Union of Geodesy and Geophysics (IUGG)
EPOS EUROPEANPLATEOBSERVINGSYSTEM

Spatiotemporal properties of the 2011 Oichalia seismic swarm, SW Peloponnese, Greece

I. Kassaras[(1)], A. Karakonstantis[(1)], V. Kapetanidis[(1)], V. Kouskouna[(1)], A. Ganas[(2)], G. Chouliaras[(2)], G. Drakatos [(2)], A. Moshou[(2)], V. Mitropoulou[(1)], P. Argyrakis[(2)], E. Lekkas[(1)], K. Makropoulos[(1)]

(1) Department of Geophysics-Geothermics, University of Athens, Panepistimiopolis, Zografou, 15784, Greece
(2) Institute of Geodynamics, National Observatory of Athens, Lofos Nymfon, 11810 Athens, Greece

Abstract

During the period between August and December 2011 a seismic swarm took place in the area of Oichalia, north Messinia province, at the southern part of Peloponnesus. The largest earthquakes occurred on 14/8/2011 (Mw=4.8) and 10/10/2011 (Mw=4.7), followed by a large number of smaller events. The shallow seismic sequence was composed of about 1600 events and it has been studied using data from local temporary and regional permanent seismological stations to investigate the fault geometry, stress field, evolution of seismicity and seismic properties. Data were analyzed in terms of manual arrival time picking and the earthquakes were located using the HYPOINVERSE algorithm, incorporating a custom local velocity model that was calculated using an iterative error minimization procedure. Hypocentral solutions were further improved by applying the double-difference algorithm (HypoDD). Focal mechanisms were obtained by both regional moment tensor inversion and P-wave first motion polarities. The relocated seismicity forms a band as narrow as 7 km (measured approximately E-W) beneath the central part of the ground openings reported by in situ surveys, less than half as wide as the distribution reported by routine catalogue locations, with an average depth of 8.7 km. Both, spatial distribution of seismicity and focal mechanisms show that the activated fault zone is dominated by dip-slip normal faulting, trending NNW-SSE. The average T-axes orientation is N70°E. The spatio-temporal distribution of the swarm follows a NNW to SSE direction of seismic activity as a function of time, toward a large seismogenic zone, which was last activated on September 13, 1986, with an Ms=6.0 earthquake. Possible causes of the observed foci migration may be related with coseismic and/or post-seismic stress changes and diffusion of the pressurized crustal fluids, as Coulomb stress transfer and local seismic tomography results indicate.

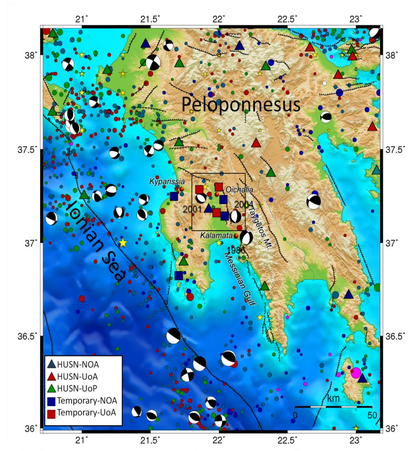

Figure 1. *Seismotectonic map of Peloponnesus. Black lines denote active boundaries and intraplate faults. Yellow stars are epicenters of historical earthquakes that occurred before 1900. Solid circles are instrumental earthquakes with origin time after the year 1900 (Ms≥4.0, Makropoulos et al., 2012). Beach-ball diagrams are CMT solutions (1976-2012). The size of epicenters and focal mechanisms is proportional to the magnitude. Solid triangles denote seismorgaphic stations used in this study.. Black rectangle bounds the study area.*

1. Introduction

SW Peloponnesus (Greece) is one of the most tectonically and seismically active areas of the Hellenic arc, due to its proximity to the Hellenic trench where oceanic lithosphere subducts beneath the Aegean microplate (Papazachos *et al.*, 2000). The convergent plate motion results in intense deformation of the crust and the release of stored elastic energy by seismic slip along large faults. A component of regional uplift is also present because of the 3-5 times higher velocity of the overriding upper plate (Aegean) in comparison to the descending African plate. Fig. 1 presents the main seismotectonic features of the broader study area.

This study is focused on a seismic swarm that took place in north Messinia, during the period between August and December 2011. The largest earthquakes that occurred on 14/8/2011 (M_w=4.8) and on 10/10/2011 (M_w=4.7) were slightly damaging to a number of houses and moderately damaging to isolated cases of old buildings of high vulnerability. In this work, we present 1) the analysis of similar earthquakes (multiplets) and their hypocentral relocation 2) the spatiotemporal analysis for the investigation of possible patterns in the evolution of the seismic swarm activity, 3) the inferred stress field by the determination of focal mechanisms 4) the stress variations as estimated by spatial mapping of differential *b*-values as well as by coulomb stress transfer caused by important events that occurred in the past and 5) the seismic velocity field deduced from travel-time tomography.

The August 2011 Oichalia swarm was recorded by the Hellenic Unified Seismological Network (HUSN). In order to improve the detectability of the smaller events, the University of Athens and the Geodynamics Institute of the National Observatory of Athens (GI-NOA) installed a local temporary network on 20 October 2011 complementary to HUSN. The combined acquisition layout recorded more than 2000 events. Automatic P-wave arrival time picking, location and maximum amplitude measurements for preliminary magnitude estimations were performed in real-time, using analysis modules implemented in the acquisition system SeisComP. During a second stage, manual picking of P- and S-wave arrival-times and measurement of signal duration were performed for events recorded by at least six stations and 1615 earthquakes were successfully located using Hypoinverse, considering a regional velocity model for the broader area of Peloponnesus. A subset of best-located aftershocks was used to extract an optimum local velocity model by applying the hypocentral location uncertainties minimization technique.

2. Multiplet analysis / Relocation Procedure

The precision of the hypocentral distribution was further improved by applying the relocation algorithm HypoDD (Waldhauser and Ellsworth, 2000). This method uses the assumption that when the distance between two events' foci is much smaller than their (common) hypocentral distance from a station, then their seismic raypaths are approximately the same and their travel-time differences can be attributed to the distance between the two foci. The algorithm works by minimizing the double-differences between observed and calculated travel-times of P- or S-waves of neighboring events at the same station, allowing for corrections of relative hypocentral positions by reducing uncertainties caused by deviations between modeled and real velocity structure. Furthermore, cross-correlation differential travel-time data can also be incorporated into the relocation procedure, providing information on waveform similarity between strongly correlated events and taking into account the arrival-time reading consistency errors.

The full waveform signals (both P- and S-wave as well as the waveform coda) of the band-pass filtered vertical component recordings of all events with available waveform data from several stations were cross-correlated to construct a combined matrix by keeping the maximum correlation value for each pair of events. Following, nearest-neighbour linkage was applied using a threshold that was selected by the empirical assumption (Kapetanidis et al., 2010) that the optimal value is the one which maximizes the difference between the size of the largest multiplet and the sum of clustered events (where "cluster size" here refers to the number of events contained in a multiplet). The calculated threshold was C_{th}=0.75 which resulted in 998 events contained in 223 multiplets. A sum of 406 events belongs to the 19 largest multiplets with size ≥10.

Following, another cross-correlation procedure was applied for every combination of pairs of events in each multiplet, performed on P- or S-waves separately on each station, with initial waveform alignment on their observed arrival-times. In each case, both the cross-correlation maximum and its corresponding time-lag were registered for each of the 3 components and weighted mean values were calculated according to the waveform type analysed in each case (P or S). The consistency between time-lag measurements and the type of component were also taken into consideration, as the P-waves are more distinctly recorded on the vertical component, while the horizontal ones are more important for S-waves.

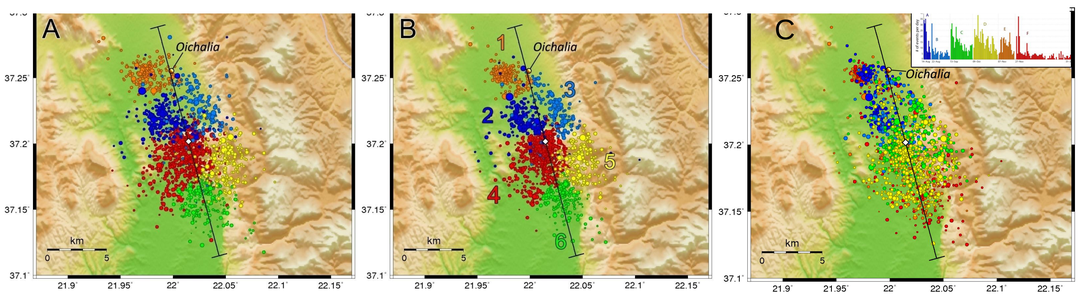

Figure 2. *Epicenters of the seismic swarm sequence A) before and B) after relocation with HypoDD. Colours and numbers (Panel B only) represent the 6 major spatial clusters that could be distinguished. The line drawn at N165°E azimuth, centered at 37.2018°N, 22.0148°E (white diamond), is used for the cross-sections of Fig. 3 C) Map of the temporal evolution of the relocated events with different colours representing the six consecutive periods in which the sequence has been divided. The embedded histogram shows the daily number of earthquakes per time-period (A-F).*

Starting with 1516 sufficiently linked events, 1480 were successfully relocated, representing 91.6% of the full catalogue data. The mean origin shift was ~22m, which is important as it shows that there is only minimal systematic shift of the hypocenters and that the events' locations were mostly concentrated closer to the main body of the original distribution or to their cluster's centroid. This result is displayed in Figures 2B and 3B in comparison to the initial locations (Figures 2A and 3A).

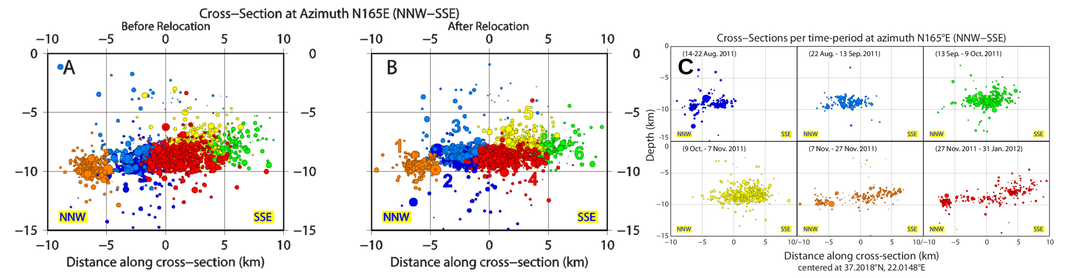

Figure 3. *Cross-section of the seismic swarm sequence at N165°E direction (NNW-SSE), centered at 37.2018°N, 22.0148°E (see Fig. 2), A) before and B) after relocation with HypoDD. Colours and numbers represent the 6 spatial clusters that were discriminated and correspond to the same colour/number labels as shown in Fig. 2, C) 6 Panels representing the different time-periods that the temporal distribution was divided at (same as in Fig. 2C): 14-22 Aug. 2011, 22 Aug. – 13 Sep. 2011, 13 Sep. – 9 Oct. 2011, 9 Oct. – 7 Nov. 2011, 7 Nov. – 27 Nov. 2011 and 27 Nov. 31 2011 – 31 Jan. 2012.*

3. Focal Mechanisms

Broadband waveform data from the HUSN were collected and analysed in order to determine the source parameters of the largest events of the Oichalia swarm. The source parameters of 7 earthquakes with magnitudes Mw ≥ 3.6 were calculated based on moment tensor inversion using regional waveforms (epicentral distances less than 3°). First motion polarity observations available from the HUSN were also incorporated. Equal area projections of the lower focal hemisphere were constructed. Focal mechanism solutions were constrained by at least six P-wave first motions. Take-off angles were computed based on the new seismic velocity model.

All 146 focal mechanism MT and P-wave first motion polarities solutions are displayed in Fig. 4. As it can be observed, the majority of focal mechanisms exhibit normal faulting. Few strike-slip and reverse focal mechanisms observed towards the southern aftershocks zone are related to the southwestern termination of the activated zone. Cross-section performed perpendicular to the activated structure imply for a normal dip-slip fault plane. Focal mechanism solutions define an average 2D plane in a least-squares sense striking N164°E. MT solutions of the largest events present an average dip angle of 37°, while those determined by P-wave first motion polarities present an average dip angle of 47° WSW.

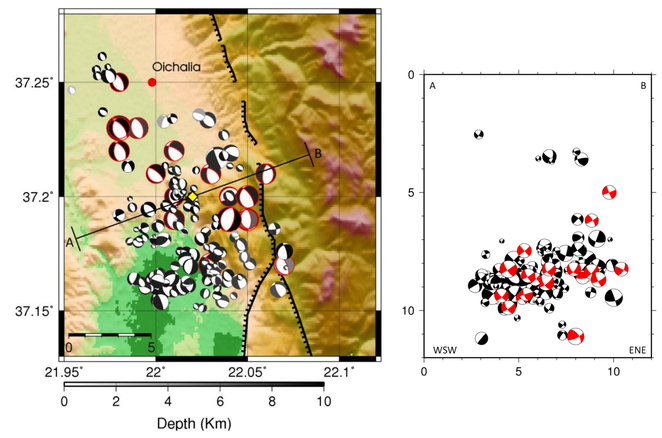

Figure 4. *(Left) All 146 focal mechanisms determined in the present study. The size of beachballs is proportional to the magnitude, which ranges between 0.4 and 4.8. Beachballs with solid circles at their centers denote regional MT solutions, while the rest denote P-wave first motion polarities solutions. The line AB, drawn in N75°E direction, centered at the white diamond, is used for the focal mechanisms cross-section of the next figure, (Right) Cross-section in AB direction, in the profile shown at the left panel. The red beachballs denote MT solutions derived using regional data, while the black ones represent mechanisms constrained with P-wave first motion polarities.*

4. b-value distribution

In this study we have determined and mapped the spatial and temporal b-value distribution in the Messinia basin using the ZMAP software (Wiemer, 2001). The b-values for two time periods, prior to and after the initiation of the seismic swarm (14 August 2011) were calculated at the nodes of a grid spacing of overlapping volumes in order to provide a natural smoothing of the results as described by Wyss and Weimer, 2000.

Fig. 5 demonstrates the b-value difference map (Δb) associated with the 2011 seismic swarm in the Messinia basin. The Δb-value map is produced by determining the difference of the b-values between the two time periods at a grid spacing of ~10 km, which contains overlapping volumes of a constant radius of 3 km and a minimum sample of 40 seismic events. The b-values for the background period prior to the initiation of the seismic swarm on 14 August 2011 were determined using the maximum likelihood method and the instrumental earthquake catalogue of NOA (from year 1964 up to 14 August 2011). For the second period, from 14 August up to its natural (bell-shape/Gaussian) decay on 31 December 2011, the b-values were determined by the same statistical method, using the relocated dataset presented in this study. A total of 2693 earthquakes with magnitudes ranging 0.4-5.5 have been used in this analysis, with about 60% belonging to the seismic swarm with better location accuracy and smaller earthquake size distribution. The obtained distribution indicates a progressive increase of stress from the northwest towards the southeast, which is consistent with the observed space/time migration of the seismicity during the 2011 swarm evolution.

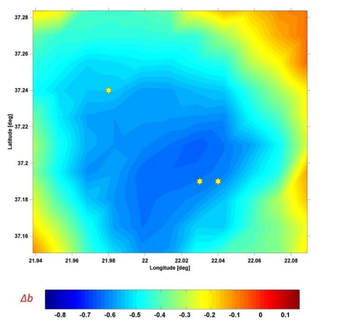

Figure 5. *(Differential b-value map and epicenters of the three largest shocks (stars) of the Messinia basin seismic swarm in 2011. The map has been determined by subtracting the b-value of the background period (1964-2011) from the 2011 swarm period, at each node of the same grid as described in section 4. Negative values indicate a relatively lower b-value for the latter (2011 swarm) period.*

5. Local traveltime tomography

In order to detect local-scale structures or other phenomena related with the geodynamics of the 2011 sequence, a travel-time tomography scheme (LOTOS, Koulakov, 2009) was employed and 3-D variations of P-, S-wave speed and Vp/Vs ratio were obtained. The LOcal TOmography Scheme takes P- and S-wave arrival times and an initial 1-D velocity model as input.

Synthetic Modeling

A difficulty commonly encountered in tomography methods is the estimation of the reliability of the obtained images. Data resolution is mainly controlled by ray-path distribution, model parameterization and smoothing. Modern inversion methods provide tools such as the a posteriori errors and the resolution matrix. However, those tools have often been found difficult to apply, hence a different approach, the checkerboard test, based on the inversion of synthetic data, has been developed. In this approach, the quality criterion is the similarity between the final model and the arbitrary model used to compute the synthetics.

A checkerboard test scheme (Koulakov, 2009) was employed in order to define the resolution of the final resolved structures. The size of the initial checkerboard cells was set according to the parameterization of the real data inversion and the expected anomalies associated with local tectonic structures. The travel-times for the source/receiver paths were computed using 3-D bending ray tracing. Following, the travel-times are perturbed with Gaussian noise generated from a predefined RMS error for P and S data. In our case, the RMS error level employed for P and S data was 0.1 and 0.15 sec, respectively.

The resulting synthetic tomograms indicate the capability of the existing ray distribution to reproduce the actual velocity structure. Synthetic tomograms are quite satisfactory, since the initial model was reconstructed successfully in a sufficient scale for the study area, for both P- and S-wave observations. More specifically, at depth slices between 2 and 12 km the initial checkerboard model was almost fully reconstructed around the area of Oichalia, allowing for the adequate interpretation of the calculated real-data tomograms.

Real-data Inversion

During the inversion process, the 1480 relocated events were included in the iterative tomography scheme, with their focal locations, P- and S-wave travel-times and ray incident angles used as input data. Limitations to the procedure might possibly arise, despite the fact that a large amount of high quality hypocentral solutions was used, as most of the events are located inside the local network.

The absence of out-of-network events imposes drastic limits to the spatial resolution of the tomographic images (Koulakov, 2009). To overcome this problem, a 190 events located off the azimuthal coverage of the local network were employed to aid the inversion procedure. 34286 rays (21008 P and 13278 S rays) were used in total, originating from a total of 1680 events foci.

Wave-speed variations generally range between +22% and -22% for P- and S-waves, while the V_p/V_s ratio varies between 1.45 and 2.20 (Fig. 6). As the synthetic modeling indicates, the speed field is adequately resolved down to the depth of 13 km. Below that level there is limited fidelity, hence the interpretation is restricted within the range 1-15 km depth.

The resulting tomograms show both strong horizontal and vertical variations. Similar configuration is observed concerning the P- and S-wave velocity anomalies, although with different magnitudes, being larger for the shear wavefield.

The 2011 swarm is restricted within a high velocity zone, surrounded by regions of low velocities (Fig. 6A). It is interesting that the low velocity zones displayed in the tomograms correlate well with significant tectonic features situated in the area; the Lower Messinia Basin and Vlachopoulo graben to the south and the Megalopolis basin and Kyparissia graben to the north. The southern structure forms a large-scale morphological depression in a NE-SW direction, perpendicular to the inferred activated fault and also perpendicular to the Taygetos Mt. (southwestern Hellenides) and the Hellenic arc.

It is noteworthy that two low velocity peak zones are observed on both sides of the Kalamata fault, which generated the 1986, M_s(NOA)=6.0 earthquake. The northern structure of Kyparissia graben is roughly sub-parallel to the southern low velocity zone. Megalopolis basin is a NW-SE structure, striking NNW-SSE, located within the Taygetos Mt. massif.

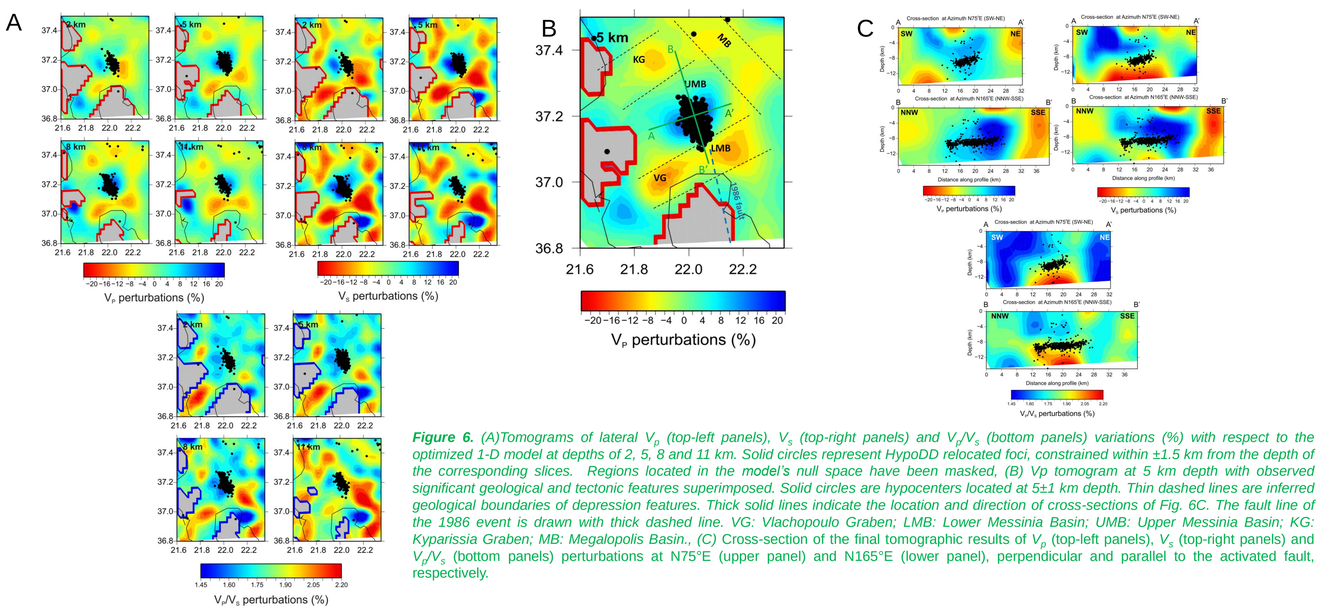

Figure 6. *(A)Tomograms of lateral V_p (top-left panels), V_s (top-right panels) and V_p/V_s (bottom panels) variations (%) with respect to the optimized 1-D model at depths of 2, 5, 8 and 11 km. Solid circles represent HypoDD relocated foci, constrained within ±1.5 km from the depth of the corresponding slices. Regions located in the model's null space have been masked, (B) Vp tomogram at 5 km depth with observed significant geological and tectonic features superimposed. Solid circles are hypocenters located at 5±1 km depth. Thin dashed lines are inferred geological boundaries of depression features. Thick solid lines indicate the location and direction of cross-sections of Fig. 6C. The fault line of the 1986 event is drawn with thick dashed line. VG: Vlachopoulo Graben; LMB: Lower Messinia Basin; UMB: Upper Messinia Basin; KG: Kyparissia Graben; MB: Megalopolis Basin., (C)* Cross-section of the final tomographic results of V_p (top-left panels), V_s (top-right panels) and V_p/V_s (bottom panels) perturbations at N75°E (upper panel) and N165°E (lower panel), perpendicular and parallel to the activated fault, respectively.

6. Coulomb stress changes

Seismic slip causes redistribution of static stress, which may in turn accelerate or delay the occurrence of other strong seismic events. The calculation of Coulomb stress changes was performed with the Coulomb 3.3 algorithm (Toda *et al.*, 2011), assuming a Poisson's ratio of 0.25 and a shear modulus of 30 GPa. Since no slip distribution models were available, unilateral ruptures were considered in all cases.

As presented in Fig. 7, only the southernmost portion of the 2011 hypocenters is located within positive stress lobes of the 1986, M_s=6.0 Kalamata earthquake. Additionally, the Coulomb stress transfer magnitude is small, less than 0.5 bars. However, the Oichalia seismic swarm was initiated with an M_w=4.8 event on 14 August 2011 at the northern part (latitude≈37.23°) where no Coulomb stress was transferred. We can therefore suggest that the epicentral area of the 2011 activity was not affected by the 1986 event. Regarding the cases of the 2001 and 2004 earthquakes, both, or a combination of both could have accelerated the occurrence of the 2011 seismic swarm, as it is included within positive lobes of Coulomb stress. The amplitude, however, of the induced stress was only about 0.5 bars, just a fraction of the stress drop of an earthquake. A stress transfer of this magnitude is too weak to trigger earthquakes, even moderate ones, like the 4.8 major shock. According to Horálek and Fischer (2008), it could be accountable for triggering only if the focal area of the RF is critically loaded. This is likely the case when pressurized fluids, which increase the pore pressure and reduce the friction coefficient, bring the fault to the limit of its stability.

Lastly, we examined the case of the 14 August 2011 major shock (M_w=4.8). As with the other cases, the size of the maximum induced stress is small, ~0.5 bars. At the bottom-right panel of Fig. 7, a NW-SE cross-section, parallel to the inferred 2011 fault zone, shows that the first two temporal clusters (time period 14 August – 13 September, Fig. 2C) are located within the relaxed area of the initiating event, below the stress-loaded zone, which is restricted between 7-9 km depth. This pattern is compatible with the results of the V_s and V_p/V_s tomographic images, showing that the largest part of the swarm lies on a zone of low shear modulus *m*, implying for the presence of fluids. This might be interpreted by volumetric pressure perturbation induced by the 14 August major event, causing fluids translation at the deeper part of the seismogenic zone and enhancing shearing in the region where these temporal clusters are observed.

7. Conclusions

The analysis of seismicity of active faults has been proven a fundamental step for the study of the geometry, mechanical properties and dynamic processes of rupture zones, which are crucial parameters for the seismic hazard assessment of a seismically prone area. In this paper, we investigate the 2011 Oichalia earthquake swarm, which started on 14/8/2011 with an M_w=4.8 event and was followed by a large number of aftershocks, several of which having M_w>3.5. The pattern was quite similar to the 8 May to 20 September 1917 sequence, according to the "Annales de l' Observatoire National d'Athènes" and as the living memory of the local inhabitants recalled during an in situ survey conducted by our research group.

The reported hot springs in the broader area are delineated along major rivers (Alfeios, Neda, Pamissos). Westerly, those rivers are parallel to active Pleistocene-Quaternary faults forming the Kyparissia, Lower Messinia and Vlachopoulo basins (Fig. 6B). Easterly, rivers flow along the direction of older (Late Miocene-Pliocene) normal faults, parallel to the Hellenic arc, probably formed prior to the onset of recent (Pliocene-Quaternary) E-W normal faulting. Following this pattern, we can presume that it is mainly surface water, originating from high precipitation, which supplies the area's hot springs.

The inferred seismogenic fault of the 2011 seismic sequence is as long as 20 km, striking NNW-SSE. The average dip of the hypocenters distribution is roughly 20°WSW, while the computed focal mechanisms present an average dip of 42°WSW. Following each of the dip angle configuration, two cases are likely possible:

1) Taking into consideration the low-angle of 20°WSW, a major rupture plane is defined, which if extrapolated to the surface is situated some 12 km east of the swarm, apparently projected within an area dominated by the Alpine basement formations and the core of the tectonic horst north of Taygetos Mt. The inferred structure lies along Alfeios River, at the western ramps of Taygetos Mt. The scarp of a segment of this fault (about 10 km long) has been observed and mapped by Armijo *et al.* (1992).

2) Taking into account the focal mechanisms average dip of 42°WSW, we could presume that more than one structures are involved, interacting with each other, forming a complex fault network which is compatible with the tectonic graben of Oichalia, part of the dominant gross Upper Messinia graben. The activation of numerous small faults may explain both the observed ground openings at the village Siamo, the generation of water hot springs above the hypocentral volume and the inhomogeneous distribution of macroseismic intensities across the meizoseismal area.

According to the relocated spatiotemporal distribution, this swarm was initiated north of Oichalia, beneath the Loutro sulfide thermal spring and propagated towards the SSE, with a rate of ~80 m/day. A local disturbance of the deep hydrostatic pressure, caused by an abrupt change in the extensional stress field during the mainshock of 14/8/2011, further activating a water volumetric pulse could possibly interpret the implications. Water, penetrating through the (older, Late Miocene-Pliocene) NNW-SSE fracture zone, enhanced progressive shearing towards the SSE, by decreasing the friction coefficient and consequently increasing the effective stress. According to Colletini and Holdsworth (2004) crustal fluids could react with crushed cataclasites at grain scale, which lead to fault alteration and to its weakening, stimulating shearing across the rupture plane. This efficiently explains the long duration of the swarm (similarly to the 1917 pattern), despite its quite small-size major events (M_w≤4.8), as well as the inferred seismic activity migration.

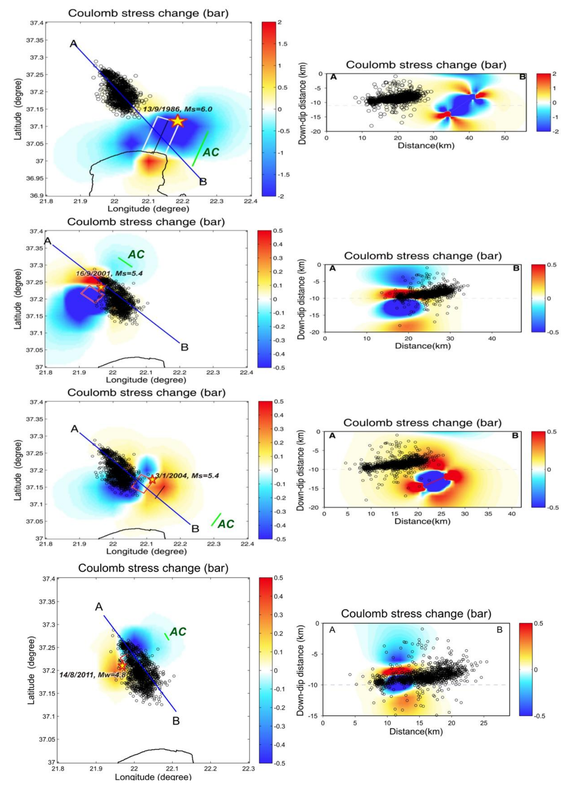

Figure 7. *Coulomb stress transfer due to the major events in the area. The active fault's projection to the surface is denoted by a thick line marked with "AC". Rectangles denote the rupture area. Black circles are the 2011 relocated events. Stress changes are presented on RF resolved by the average MT focal mechanisms and the hypocentral distribution. "Stress-loaded" or "relaxed" areas are represented in the colour scale by positive or negative values, respectively. Black circles are the relocated aftershocks. Right: Coulomb stress transfer cross-sections along AB profile, parallel to the RF.*

Acknowledgments

The present study was funded through the 7th FP project "EPOS: European Plate Observing System" which is the integrated solid Earth Sciences research infrastructure approved by the European Strategy Forum on Research Infrastructures (ESFRI) and is included in the ESFRI Roadmap. It was partly financed by the XENIOS Project (09ΣΥΝ-31-867), coordinated by the Greek Ministry of Research and Technology and the LACAE, Faculty of Geology and Geoenvironment, NKUA and SARG-UoA. We are grateful to Administration of Peloponnesus and Local Authorities.

8. References

Armijo, R., H. Lyon-Caen, D. Papanastassiou, 1992. East-west extension and Holocene normal-fault scarps in the Hellenic Arc, *Geology*, 20(6), 491 – 494, doi:10.1130/0091-7613.
Colletini, C., Holdsworth, R.E., 2004. Fault zone weakening and character of slip along low-angle normal fault: insights from the Zuccale fault, Elba, Italy. J. Geol. Soc. London, 161, 1039-1051.
Horálek, J. and Fischer, T., 2008. Role of crustal fluids in triggering the West Bohemia/Vogtland earthquake swarms. Just what we know (A review), Stud. Geophys. Geod., 52, 455-478.
Kapetanidis, V., Papadimitriou, P., Makropoulos, K., 2010. A cross-correlation technique for relocation of seismicity in the western Corinth rift. *Bull. Geol. Soc. Greece*, Proc. of the 12th International Congress, Patras, May 2010, XLIII, No 4, p. 2015-2025
Koulakov, I., 2009. LOTOS code for local earthquake tomographic inversion. Benchmarks for testing tomographic algorithms, *BSSA*, Vol. 99, No. 1, pp. 194-214.
Papazachos, B. C., Karakostas, V.G., Papazachos, C.B.,, Scordilis, E.M., 2000. The geometry of the Wadati-Benioff zone and lithospheric kinematics in the Hellenic Arc, Tectonophysics, 319(4), 275–300, doi:10.1016/S0040-1951(99)00299-1.
Toda, S., Stein, R.S., Sevilgen, V. and Lin, J., 2011, Coulomb 3.3 Graphic-rich deformation and stress-change software for earthquake, tectonic, and volcano research and teaching—user guide: U.S. Geological Survey Open-File Report 2011-1060, 63 pp.
Waldhauser, F., Ellsworth, W.L., 2000. A double-difference earthquake location algorithm: method and application to the northern Hayward fault, Bull. Seism. Soc. Am., 90, 1353–1788.
Wiemer, S., 2001. A software package to analyze seismicity: ZMAP, Seismol. Res. Lett., 72, 374–383.
Wyss, M., Wiemer, S., 2000. Change in the Probability for earthquakes in Southern California Due to the Landers Magnitude 7.3 Earthquake, Nature, 290, 1334–1338.